Structural, Spectroscopic, and Magnetochemical Characterization of the Trinuclear Vanadium(III) Carboxylates [V₃O(O₂CR)₆L₃](ClO₄) (R = Various Groups; L = Pyridine, 4-Picoline, 3,5-Lutidine)

Stephanie L. Castro, William E. Streib, Jui-Sui Sun, and George Christou*

Department of Chemistry and Molecular Structure Center, Indiana University, Bloomington, Indiana 47405-4001

Synthetic procedures are described that allow access to the $[V_3O(O_2CR)_6L_3](ClO_4)$ (R = various groups; L = pyridine (py), 4-picoline (pic) or 3,5-lutidine (lut)) family of complexes. Treatment of $VCl_3(THF)_3$ with NaO_2-CR (R = Me, Et) in RCO_2H/py, pic/MeCN, or CH_2Cl_2 solution followed by addition of $NBu^n_4ClO_4$ leads to isolation of $[V_3O(O_2CR)_6L_3](ClO_4)$ salts in 47−95% yields. A similar procedure for R = C_6H_5, C_6H_4-p-OMe, C_6H_3-m-Me₂, and C_6H_4-p-Cl but omitting addition of NaO_2CR provides the corresponding benzoate or substituted-benzoate derivatives in 24−56% yields. The X-ray structure of $[V_3O(O_2CEt)_6(pic)_3](ClO_4)$ (**4**) shows the anion to consist of a $[V_3O]^{7+}$ triangular fragment with a μ_3-O^{2-} ion in the V_3 plane; each triangular edge is bridged by two $EtCO_2^-$ groups in their familiar *syn,syn* modes, and there is a terminal pic group on each V^{III} completing distorted octahedral geometries at the metal atoms. The cation has imposed C_2 symmetry (isosceles V_3 triangle), the C_2 axis passing through one V atom and the central μ_3-O atom, but has D_{3h} virtual symmetry (equilateral V_3 triangle). Complex **4** crystallizes in monoclinic space group $C2/c$ with the following unit cell dimensions at −171 °C: $a = 13.935(2)$ Å, $b = 18.323(2)$ Å, $c = 17.470(2)$ Å, $\beta = 95.55(1)°$, $V = 4439.7$ Å³, $Z = 4$. The structure was solved using 2657 unique reflections with $F > 3\sigma(F)$ and refined on F to conventional R (R_w) values of 0.058 (0.066). Variable-temperature, solid-state magnetic susceptibility measurements were made on complex **1** in the 5.01−280 K region in a 1 kG magnetic field. The effective magnetic moment (μ_{eff}) per V_3 unit decreases gradually from 4.64 μ_B at 280 K to 1.76 μ_B at 5.01 K. The data were fit to the theoretical expression for an isosceles V^{III}_3 complex, and the fitting parameters were $J = -18.0(7)$ cm⁻¹, $J' = -10.4(4)$ cm⁻¹, and $g = 1.985$, with TIP held constant at 600×10^{-6} cm³ mol⁻¹; J' refers to the unique exchange interaction within the isosceles triangle. The ground state of complex **1** thus has $S = 0$.

Introduction

We have for several years been interested in the structural, physical, and spectroscopic properties of vanadium complexes of various nuclearities and at a variety of oxidation levels.[1] This interest derives from the occurrence of often large amounts of vanadium impurities in crude oils.[2] These impurities are of two types, the vanadyl (VO^{2+}) porphyrins[3] and the so-called vanadyl non-porphyrins:[4] study of the latter type by EPR spectroscopy reveals a family of complexes involving N, S, and/or O ligation. During crude oil upgrading, these impurities are converted to insoluble vanadium sulfides (primarily V_2S_3 and V_3S_4) by the sulfide-rich and reducing conditions of the hydro-treating processes.[5−9] Although V sulfides are autocatalytic and therefore advantageous for hydrodemetalation (HDM),[7] i.e., removal of more V from the crude, the formation of V sulfides in V-rich crudes represents a serious problem for hydrodesulfurization (HDS) and hydrodenitrification (HDN) processes because these sulfides deposit on the heterogeneous HDS/HDN catalyst employed (for example, Mo/Co/S on alumina) and lower its activity by pore-plugging, eventually deactivating it completely.[7]

The conversion of vanadyl impurities to vanadium sulfide polymers under processing conditions is not well understood but must involve the progressive deoxygenation, reduction, sulfiding, and aggregation of the V species, not necessarily in that order. Initial reduction to V^{III} and partial deoxygenation could yield oxide-bridged oligonuclear species, and for this reason, we have been interested in preparing and studying such species in the past. In the present work, we have also

⊗ Abstract published in *Advance ACS Abstracts,* July 1, 1996.
(1) Recent publications: (a) Reynolds, J. G.; Sendlinger, S. C.; Murray, A. M.; Huffman, J. C.; Christou, G. *Inorg. Chem.* **1995,** *34,* 5745. (b) Dean, N. S.; Bartley, S. L.; Streib, W. E.; Lobkovsky, E. B.; Christou, G. *Inorg. Chem.* **1995,** *34,* 1608. (c) Rambo, J. R.; Bartley, S. L.; Streib, W. E.; Christou, G. *J. Chem. Soc., Dalton Trans.* **1994,** 1813. (d) York, K. A.; Folting, K.; Christou, G. *J. Chem. Soc., Chem. Commun.* **1993,** 1563. (e) Dean, N. S.; Folting, K.; Lobkovsky, E. B.; Christou, G. *Angew. Chem., Int. Ed. Engl.* **1993,** *32,* 594. (f) Castro, S. L.; Martin, J. D.; Christou, G. *Inorg. Chem.* **1993,** *32,* 2978. (g) Sendlinger, S. C.; Nicholson, J. R.; Lobkovsky, E. B.; Huffman, J. C.; Rehder, D.; Christou, G. *Inorg. Chem.* **1993,** *32,* 204. (h) Heinrich, D. D.; Folting, K.; Huffman, J. C.; Reynolds, J. G.; Christou, G. *Inorg. Chem.* **1991,** *30,* 300. (i) Heinrich, D. D.; Huffman, J. C.; Folting, K.; Streib, W. E.; Christou, G. *J. Chem. Soc., Chem. Commun.* **1989,** 1411. (j) Rambo, J. R.; Eisenstein, O.; Huffman, J. C.; Christou, G. *J. Am. Chem. Soc.* **1989,** *111,* 8027. (k) Christou, G.; Folting, K.; Huffman, J. C.; Heinrich, D. D.; Rambo, J. R.; Money, J. K. *Polyhedron* **1989,** *8,* 1723. (l) Money, J. K.; Huffman, J. C.; Christou, G. *Inorg. Chem.* **1988,** *27,* 507.
(2) Yen, T. F. *The Role of Trace Elements in Petroleum*; Ann Arbor Science: Ann Arbor, MI, 1975; Chapter 1.
(3) Sundararaman, P. *Anal. Chem.* **1985,** *57,* 2204.
(4) Reynolds, J. G.; Gallegos, E. J.; Fish, R. H.; Komlenic, J. J. *Energy Fuels* **1987,** *1,* 36.

(5) Silbernagel, B. G.; Mohan, R. R.; Singhal, G. H. *ACS Symp. Ser.* **1984,** *248,* 91.
(6) Silbernagel, B. G. *J. Catal.* **1979,** *56,* 315.
(7) Asaoka, S.; Nakata, S.; Shiroto, Y.; Takeuchi, C. *ACS Symp. Ser.* **1987,** *344,* 275.
(8) Rose-Brussin, M.; Moranta, D. *Appl. Catal.* **1984,** *11,* 85.
(9) Mitchell, P. C. H.; Scott, C. E.; Bonnelle, J.-P.; Grimblot, J. G. *J. Chem. Soc., Faraday Trans. 1* **1985,** *81,* 1047.
(10) Fish, R. H.; Reynolds, J. G.; Gallegos, E. J. *ACS Symp. Ser.* **1987,** *344,* 332.
(11) Seifert, W. K. *Prog. Chem. Org. Nat. Prod.* **1975,** *32,* 1.

incorporated carboxylate groups because (i) this is an organic functionality identified in crude oils[10,11] and (ii) the O-based ligands suggested by EPR data on the vanadyl non-porphyrins most likely include carboxylates.[10] Thus, we have sought to prepare oxide-bridged V^{III} carboxylate species of various nuclearities to model an initial fate of vanadyl species in crude oils from reduction/partial deoxygenation/aggregation steps. In this report, we concentrate on trinuclear V^{III} carboxylate complexes. Preliminary results at the tetranuclear level have been communicated elsewhere.[12]

Vanadium(III) carboxylates have attracted some prior interest, primarily by Cotton and co-workers, who prepared the trinuclear species $[V_3O(O_2CMe)_6(MeCO_2H)_2(THF)][VCl_4(MeCO_2H)]$,[13a] $[V_3O(O_2CCH_2Cl)_6(H_2O)_3](CF_3SO_3)$,[13b] and $[V_3O(O_2CMe)_6$-$(THF)_3]/[V_2O_2Cl_6]$;[13b] this group also prepared V^{II}, $2V^{III}$,[13a] and $3V^{IV}$ [14] analogues (as well as the octanuclear heterometallic species $Zn_4V_4O_4(O_2CR)_{12}(THF)_4$[15]). The $3V^{III}$ species all contain a triangular, oxide-centered unit. Using these prior observations as a starting point and seeking (i) to incorporate terminal py groups as an ^1H NMR handle and (ii) to avoid the presence of paramagnetic anions that would complicate magnetochemical studies, we have sought the preparation of trinuclear V^{III} carboxylates in high yield and purity, with readily variable carboxylate groups and with diamagnetic anions. We herein report the successful development of a general synthetic route to $[V_3O(O_2CR)_6L_3](ClO_4)$ complexes, together with structural, physical, and spectroscopic characterization of representative examples.

Experimental Section

Syntheses. All manipulations were carried out under a dinitrogen atmosphere using standard Schlenk and glovebox techniques. Solvents were distilled before use from CaH_2 (MeCN) or Na/benzophenone (Et$_2$O, THF). $VCl_3(THF)_3$[16] was prepared as described elsewhere: py = pyridine; pic = 4-picoline = 4-methylpyridine; lut = 3,5-lutidine = 3,5-dimethylpyridine.

$[V_3O(O_2CMe)_6(py)_3](ClO_4)$ (1). $VCl_3(THF)_3$ (4.86 g, 13.0 mmol) and anhydrous NaO_2CMe (3.2 g, 39 mmol) were slowly dissolved with stirring over 24 h in a solvent mixture of MeCN (40 mL), $MeCO_2H$ (20 mL), and pyridine (40 mL). The resultant deep green solution was filtered to remove NaCl, and $NBu^n_4ClO_4$ (1.5 g, 4.4 mmol) was added to the filtrate. The volume of the solution was decreased *in vacuo* until a green powder began to appear, and Et$_2$O (75 mL) was added, resulting in precipitation of a large quantity of green microcrystalline solid. This was collected by filtration, washed copiously with Et$_2$O (3 × 100 mL) to remove traces of acetic acid and pyridine, and dried *in vacuo*. The yield of complex **1** was 3.53 g (95%). Anal. Calcd (found) for $C_{27}H_{33}N_3O_{17}ClV_3$: C, 37.78 (37.85); H, 3.88 (3.98); N, 4.90 (4.67). Electronic spectrum in MeCN, λ_{max}, nm (ϵ_M, L mol^{-1} cm^{-1}): 204 (16 254), 246 (11 405), 322 (1512), 430 (670), 584 (443).

$[V_3O(O_2CMe)_6(pic)_3](ClO_4)$ (2). The procedure for complex **1** was followed, employing $VCl_3(THF)_3$ (1.12 g, 3.00 mmol) and NaO_2CMe (0.74 g, 9.0 mmol) in a mixture of MeCN (20 mL), $MeCO_2H$ (10 mL), and 4-picoline (22 mL), followed by addition of $NBu^n_4ClO_4$ (0.34 g, 1.0 mmol) to the green filtrate and precipitation of the product with Et$_2$O (100 mL). The yield of green crystalline solid was 0.82 g (91%), and it analyzed as **2**·$^1/_3$Et$_2$O. Anal. Calcd (found) for $C_{31.32}H_{42.3}$-$N_3O_{17.33}ClV_3$: C, 40.61 (40.70); H, 4.60 (4.60); N, 4.54 (4.56).

$[V_3O(O_2CMe)_6(lut)_3](ClO_4)$ (3). The procedure for complex **1** was followed, employing the reagents and amounts indicated in the

procedure for complex **2**, except that 4-picoline was replaced with 3,5-lutidine (20 mL). The green microcrystalline solid was impure, as indicated by ^1H NMR spectroscopy, and two recrystallizations from MeCN/Et$_2$O were performed. The overall yield was 0.55 g (54%), and the solid analyzed as **3**·$^2/_3$lut. Anal. Calcd (found) for $C_{37.67}H_{51}$-$N_{3.67}O_{17}ClV_3$: C, 44.55 (44.45); H, 5.06 (5.08); N, 5.06 (5.04).

$[V_3O(O_2CEt)_6(pic)_3](ClO_4)$ (4). $VCl_3(THF)_3$ (0.747 g, 2.00 mmol) was dissolved with stirring in a mixture of $EtCO_2H$ (10 mL), 4-picoline (5 mL), and CH_2Cl_2 (20 mL). The next day the solution was filtered. $NBu^n_4ClO_4$ (0.25 g, 0.73 mmol) was added to the green filtrate, and Et$_2$O was added slowly with stirring to give a white precipitate (identified as picH$^+$Cl$^-$ by ^1H NMR and IR spectroscopies and by a Ag$^+$ test for Cl). When no more white crystals were being precipitated, addition of Et$_2$O was discontinued, the solution filtered, and the filtrate stored undisturbed for 24 h, during which green, X-ray-quality crystals formed. These were collected by filtration, washed with Et$_2$O, and dried *in vacuo*. (Occasionally, small amounts of white crystals were observed contaminating the green crystals; these could be removed by washing with H$_2$O (10 mL) and Et$_2$O (50 mL), in which the product is insoluble.) The yield was 0.31 g (47%). A higher yield was subsequently obtained using the same reagent amounts but in a solvent mixture comprising $EtCO_2H$ (2 mL), 4-picoline (1 mL), and acetone (10 mL). The yields were typically 0.45 g (68%). Anal. Calcd (found) for $C_{36}H_{51}N_3O_{17}ClV_3$: C, 43.85 (44.25); H, 5.21 (5.20); N, 4.26 (4.07).

$[V_3O(O_2CC_6H_4\text{-}p\text{-OMe})_6(pic)_3](ClO_4)$ (5). The above procedure for complex **4** was followed, employing $VCl_3(THF)_3$ (0.747 g, 2.00 mmol) and anisic acid (1.52 g, 10.0 mmol) in 4-picoline (1 mL) and acetone or MeCN (10 mL). The yield was 0.56 g (56%). The dried solid analyzed for **5**·$^1/_2$pic. Anal. Calcd (found) for $C_{69}H_{66.5}N_{3.5}O_{23}$-$ClV_3$: C, 55.21 (55.03); H, 4.47 (4.52); N, 3.27 (3.28). Use of NBu^n_4-CF_3SO_3 or $NBu^n_4PF_6$ in place of $NBu^n_4ClO_4$ allowed isolation of the corresponding salts of the cation of **5**, both in ~30% yield.

The complexes $[V_3O(O_2CPh)_6(pic)_3](ClO_4)$ (6), $[V_3O(O_2CC_6H_4\text{-}p\text{-}$ Me$)_6(pic)_3](ClO_4)$ (7), and $[V_3O(O_2CC_6H_4\text{-}p\text{-Cl})_6(pic)_3](ClO_4)$ (8) were prepared according to the procedure for complex **5**, employing the corresponding carboxylic acid and MeCN (6) or CH_2Cl_2 (7 and 8); the yields of **6**−**8** were 33, 24, and 25%, respectively. The purity of the complexes was confirmed by ^1H NMR spectroscopy.

X-ray Crystallography and Structure Solution. Data were collected on complex **4** using a Picker four-circle diffractometer; details of the diffractometry, low-temperature facilities, and computational procedures employed by the Molecular Structure Center are available elsewhere.[17] The structure was solved by direct methods (MULTAN78) and standard Fourier techniques and refined on *F* by full-matrix least-squares cycles.

A suitable crystal was located, affixed to a glass fiber with silicone grease, and transferred to a goniostat where it was cooled to −171 °C for characterization and data collection. A systematic search of a limited hemisphere of reciprocal space revealed a *C*-centered monoclinic cell. Following complete intensity data collection ($+h,+k,\pm l$; 6° ≤ 2θ ≤ 45°), the additional condition $l = 2n$ for h0l limited the space group to *Cc* or *C2/c*. The choice of *C2/c* was later proven correct by the successful solution of the structure. After correction for absorption (program AGNOST), data processing produced a unique set of 2916 intensities and gave a residual of 0.018 for the averaging of 1589 reflections that had been measured more than once. Four standards measured every 300 data showed no significant trends. The positions of 22 of the 35 non-hydrogen atoms in the asymmetric unit were obtained from an initial *E*-map. The positions of the remaining non-hydrogen atoms were obtained from subsequent iterations of least-squares refinement followed by a difference Fourier map calculation. Hydrogen atoms were included in fixed calculated positions with thermal parameters fixed at 1 plus the isotropic thermal parameter of the carbon atom to which each was bonded. In the final cycles of refinement, the non-hydrogen atoms were varied with anisotropic thermal parameters to give a final $R(F) = 0.058$ for the 297 total variables using all of the unique data. Data having $F < 3\sigma(F)$ were given zero weight. The final difference Fourier map was essentially featureless, the largest peak being 0.46 and the deepest hole −0.55 e/

(12) Castro, S. L.; Sun, Z.; Bollinger, J. C.; Hendrickson, D. N.; Christou, G. *J. Chem. Soc., Chem. Commun.* **1995**, 2517.
(13) (a) Cotton, F. A.; Lewis, G. E.; Mott, G. N. *Inorg. Chem.* **1982**, *21*, 3316. (b) Cotton, F. A.; Extine, M. W.; Falvello, L. R.; Lewis, D. B.; Lewis, G. E.; Murillo, C. A.; Schwotzer, W.; Tomas, M.; Troup, J. M. *Inorg. Chem.* **1986**, *25*, 3505.
(14) Cotton, F. A.; Lewis, G. E.; Mott, G. N. *Inorg. Chem.* **1982**, *21*, 3127.
(15) Cotton, F. A.; Duraj, S. A.; Roth, W. J. *Inorg. Chem.* **1984**, *23*, 4042.
(16) Manzer, L. E. *Inorg. Synth.* **1982**, *21*, 138.

(17) Chisholm, M. H.; Folting, K.; Huffman, J. C.; Kirkpatrick, C. C. *Inorg. Chem.* **1984**, *23*, 1021.

Table 1. Crystallographic Data for $[V_3O(O_2CEt)_6(pic)_3](ClO_4)$ (**4**)

empirical formula	$C_{36}H_{51}N_3O_{17}ClV_3$	space group	$C2/c$
a, Å	13.935(2)	T, °C	-171 °C
b, Å	18.323(2)	λ, Å	0.710 69
c, Å	17.470(2)	ρ_{calcd}, g cm^{-3}	1.475
β, deg	95.55(1)	μ(Mo Kα), cm^{-1}	7.279
V, Å^3	4439.7	$R(F)^a$	0.058
Z	4	$R_w(F)^b$	0.066
fw	986.09		

^{a} $R = \sum||F_o| - |F_c||/\sum|F_o|$. ^{b} $R_w = [\sum w(|F_o| - |F_c|)^2/\sum w|F_o|^2]^{1/2}$ where $w = 1/\sigma^2(|F_o|)$.

Å^3. The cation lies on a crystallographic C_2 axis through atoms C(23), C(22), N(19), V(1), and O(3). The ClO_4^- anion is disordered in two positions about the C_2 axis, each with half-occupancy. Final values of R and R_w are listed in Table 1.

Physical Studies. Infrared and electronic spectra were recorded on Nicolet 510P and Hewlett Packard 8452A spectrophotometers, respectively. ^{1}H NMR spectra were obtained on a Varian XL300 instrument. Electrochemical measurements were performed in CH$_2$Cl$_2$/0.1 M NBu$^n_4$-ClO$_4$ at room temperature using a BAS CV50W voltammetric analyzer, a glassy carbon working electrode, a Pt wire auxiliary electrode, and an SCE reference electrode. Potentials are quoted *vs* the ferrocene/ferrocenium couple ($+0.52$ V *vs* SCE). Variable-temperature magnetic susceptibility measurements were obtained at Michigan State University with a Quantum Design MPMS SQUID susceptometer operating with a 10 kG (1 T) applied magnetic field. The experimental magnetic susceptibilities were corrected for the diamagnetic response using Pascal's constants.

Results

Syntheses. The simplest procedure that seemed a possible route to high yields of $[V_3O(O_2CR)_6(py)_3]^+$ complexes was to treat a convenient V^{III} source with an excess of a carboxylate/carboxylic acid and pyridine in a suitable organic solvent, hoping that the high oxophilicity of V^{III} would result in incorporation of an O^{2-} derived from adventitious H$_2$O (or other potential oxide sources). This approach proved successful. Thus, treatment of VCl$_3$(THF)$_3$ with NaO$_2$CMe in MeCO$_2$H/py/MeCN slowly gave deep green solutions from which was isolated $[V_3O(O_2CMe)_6(py)_3](ClO_4)$ (**1**) in ~95% yield after addition of ClO$_4^-$ ions. The preparation is summarized in eq 1, assuming

$$3VCl_3 + 9NaO_2CMe + 3py + H_2O \rightarrow$$
$$[V_3O(O_2CMe)_6(py)_3]^+ + 9NaCl + 2MeCO_2H +$$
$$MeCO_2^- \quad (1)$$
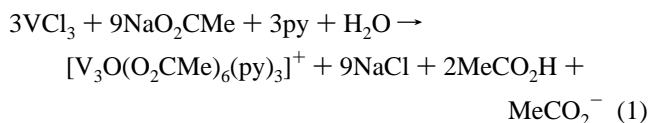
H$_2$O to be the oxide source. The presence of an excess of acetic acid was important for high yields. Essentially the same procedure was employed to prepare the 4-picoline (**2**), 3,5-lutidine (**3**), and propionate (**4**) versions of **1**, and no doubt it could be extended to other derivatives. For the benzoate (**6**) and substituted-benzoate (**5**, **7**, **8**) versions, we employed a slightly modified procedure that omitted the addition of NaO$_2$-CR; this avoided the need to synthesize the latter salts. The substituted-benzoate complexes prepared were those that were most needed for the ^{1}H NMR studies, but others are undoubtedly also accessible by this route.

Description of Structure. Complex **4** crystallizes in monoclinic space group $C2/c$. An ORTEP representation of the cation is shown in Figure 1, fractional coordinates and isotropic thermal parameters are listed in Table 2, and selected bond lengths and angles are listed in Table 3. The cation of **4** lies on a crystallographic 2-fold rotation axis containing atoms V(1), O(3), N(19), C(22), and C(23), the last two being the *p*-C and *p*-Me atoms of the picoline group containing N(19). The crystallographic symmetry of the cation is thus C_2. The
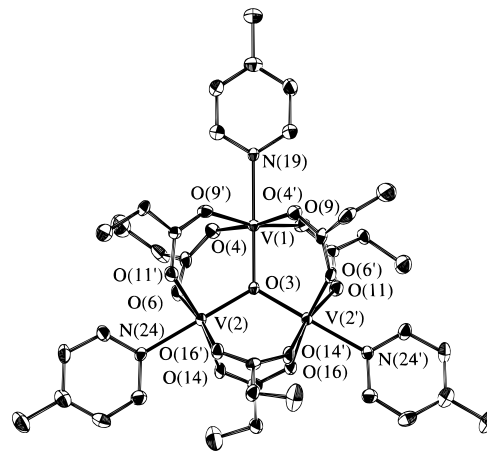
Figure 1. ORTEP representation of the cation of complex **4** at the 50% probability ellipsoid level. Primed and unprimed atoms are related by the 2-fold rotation axis through O(3), V(1), and N(19).

Table 2. Selected Fractional Coordinates ($\times 10^4$) and Equivalent Isotropic Thermal Parameters^a (Å^2, $\times 10$) for Complex **4**

atom	x	y	z	B_{eq}
V(1)	10000*	671(1)	7500*	11
V(2)	10989(1)	$-908(1)$	7033(1)	12
O(3)	10000*	$-383(3)$	7500*	12
O(4)	11405(3)	736(2)	7922(2)	17
C(5)	12094(4)	293(3)	7912(3)	16
O(6)	12044(3)	$-316(2)$	7570(2)	16
C(7)	13063(5)	515(4)	8292(4)	26
C(8)	13621(6)	949(5)	7748(6)	45
O(9)	9618(3)	795(2)	8565(2)	17
C(10)	9225(4)	395(3)	9041(3)	13
O(11)	9025(3)	$-266(2)$	8914(2)	17
C(12)	9040(4)	724(3)	9790(3)	16
C(13)	8436(5)	282(4)	10293(4)	27
O(14)	11194(3)	$-1646(2)$	7882(2)	18
C(15)	10737(4)	$-1842(3)$	8427(3)	16
O(16)	9926(3)	$-1585(2)$	8565(2)	16
C(17)	11151(5)	$-2432(3)$	8961(3)	19
C(18)	12202(5)	$-2579(5)$	8925(4)	36
N(19)	10000*	1875(4)	7500*	13
C(20)	9316(4)	2254(3)	7812(3)	16
C(21)	9302(5)	3006(4)	7812(4)	23
C(22)	10000*	3398(5)	7500*	22
C(23)	10000*	4218(5)	7500*	34
N(24)	12115(3)	$-1487(3)$	6511(3)	14
C(25)	12791(4)	$-1133(3)$	6165(4)	19
C(26)	13482(4)	$-1482(4)$	5780(4)	22
C(27)	13511(5)	$-2244(4)$	5772(3)	21
C(28)	12833(5)	$-2607(3)$	6149(4)	22
C(29)	12155(5)	$-2223(3)$	6496(4)	20
C(30)	14258(5)	$-2644(4)$	5380(4)	32

^{a} $B_{eq} = (4/3)\sum\sum B_{ij}a_ia_j$. ^{b} Parameters marked with an asterisk were fixed by symmetry.

accompanying ClO$_4^-$ anion lies in a general position and is therefore necessarily disordered about the C_2 axis with 50% occupancy at each position. The cation consists of a rigorously planar (by symmetry) [V$_3$O]$^{7+}$ triangular unit containing V^{III} atoms with distorted octahedral geometry. The V$_3$ triangle is crystallographically isosceles but virtually equilateral, with the V$\cdot\cdot$V distances (3.336(2), 3.340(2) Å) and V$-$O(3)$-$V angles (119.98(14), 120.04(28)°) insignificantly different. Peripheral ligation is provided by six bridging EtCO$_2^-$ and three terminal picoline groups to yield a cation with C_2 crystallographic symmetry but D_{3h} virtual symmetry. The cation of **4** is a new member of the venerable class of complexes with the "basic metal carboxylate" structure observed previously for many metals,[18,19] including V^{III}; the metric parameters for **4** are similar to those for other [V$_3$O(O$_2$CR)$_6$]$^+$-containing species.[13,14] It is

Table 3. Selected Bond Distances (Å) and Angles (deg) for Complex **4**

(a) Bonds			
V(1)−O(3)	1.931(5)	V(1)··V(2)	3.340(2)
V(1)−O(4)	2.028(4)	V(2)··V(2')	3.336(2)
V(1)−O(9)	1.996(4)	V(2)−O(11')	2.029(4)
V(1)−N(19)	2.205(7)	V(2)−O(14)	2.007(4)
V(2)−O(3)	1.926(3)	V(2)−O(16')	1.999(4)
V(2)−O(6)	1.987(4)	V(2)−N(24)	2.167(5)

(b) Angles			
O(3)−V(1)−O(4)	93.37(12)	O(3)−V(2)−N(24)	179.25(18)
O(3)−V(1)−O(9)	96.50(12)	O(6)−V(2)−O(11')	90.97(17)
O(3)−V(1)−N(19)	180	O(6)−V(2)−O(14)	88.50(17)
O(4)−V(1)−O(4')	173.26(24)	O(6)−V(2)−O(16')	171.99(17)
O(4')−V(1)−O(9)	89.85(17)	O(6)−V(2)−N(24)	86.17(17)
O(4)−V(1)−O(9)	89.39(17)	O(11')−V(2)−O(14)	169.37(17)
O(4)−V(1)−N(19)	86.63(12)	O(11')−V(2)−O(16')	88.72(17)
O(9)−V(1)−O(9')	167.00(24)	O(11')−V(2)−N(24)	83.74(17)
O(9)−V(1)−N(19)	83.50(12)	O(14)−V(2)−O(16')	90.32(17)
O(3)−V(2)−O(6)	93.12(15)	O(14)−V(2)−N(24)	85.63(17)
O(3)−V(2)−O(11')	96.03(16)	O(16')−V(2)−N(24)	85.84(17)
O(3)−V(2)−O(14)	94.61(16)	V(1)−O(3)−V(2)	119.98(14)
O(3)−V(2)−O(16')	94.87(15)	V(2)−O(3)−V(2')	120.04(28)

interesting to note that the py rings are all coplanar with the [V$_3$O] plane; they are expected to be either coplanar or perpendicular to this plane to minimize steric repulsions with the carboxylate O atoms, and the coplanar disposition seen is probably just due to packing effects.

Magnetic Susceptibility Studies. Variable-temperature, solid-state magnetic susceptibility studies were performed on powdered samples of complex **1** in the temperature range 5.01−280 K in a 1000 G (0.1 T) applied magnetic field (Figure 2). The effective magnetic moment (μ_{eff}) per V$_3$ unit decreases gradually from 4.64 μ_B at 280 K to 1.76 μ_B at 5.01 K. Comparison of the high-temperature values with the spin-only value expected for a V$^{III}_3$ species containing noninteracting metal centers ($\mu_{eff} = 4.90$ μ_B) suggests the presence of antiferromagnetic exchange interactions within the anion of **1**.

On the basis of the crystal structure of **4**, the V$_3$ triangular unit within the [V$_3$O(O$_2$CR)$_6$L$_3$]$^+$ cation could be approximated as equilateral, and the three pairwise magnetic exchange interactions taken to be equal, i.e., $J_{12} = J_{12'} = J_{22'} = J$, where the subscripts refer to the metal atom labeling scheme in Figure 1. The Heisenberg spin Hamiltonian for an equilateral triangle of three spins is given by eq 2, where S_i is the spin of metal V_i.

$$\hat{H} = -2J(\hat{S}_1 \cdot \hat{S}_2 + \hat{S}_1 \cdot \hat{S}_{2'} + \hat{S}_2 \cdot \hat{S}_{2'}) \qquad (2)$$

The energies $E(S_T)$ of the resultant spin states S_T for the entire V$_3$ unit (defined as $\hat{S}_T = \hat{S}_1 + \hat{S}_2 + \hat{S}_{2'}$) are given in eq 3, where

$$E(S_T) = -J[S_T(S_T + 1) - 3S(S + 1)] \qquad (3)$$

$S = S_1 = S_2 = S_{2'} = 1$. For an antiferromagnetically-coupled system ($J < 0$), this model predicts a $S_T = 0$ ground state with

(18) For reviews of trinuclear carboxylate-bridged complexes, see: (a) Mehrotra, R. C.; Bohra, R. *Metal Carboxylates*; Academic Press: London, 1983; Chapter 3.2.3. (b) Cannon, R. D.; White, R. P. *Prog. Inorg. Chem.* **1988**, *36*, 195.

(19) (a) Ohto, A.; Sasaki, Y.; Ito, T. *Inorg. Chem.* **1994**, *33*, 1245. (b) Cannon, R. D.; Jayasooriya, U. A; Montri, L.; Saad, A. K.; Karu, E.; Bollen, S. K.; Sanderson, W. R.; Powell, A. K.; Blake, A. B. *J. Chem. Soc., Dalton Trans.* **1993**, 2005. (c) Almog, O.; Bino, A.; Garfinkel-Shweky, D. *Inorg. Chim. Acta* **1993**, *213*, 99. (d) Jang, H. G.; Geib, S. J.; Kaneko, Y.; Nakano, M.; Sorai, M.; Rheingold, A. L.; Montez, B.; Hendrickson, D. N. *J. Am. Chem. Soc.* **1989**, *111*, 173. (e) Anson, C. E.; Chai-Sáard, N.; Bourke, J. P.; Cannon, R. D.; Jayasooriya, U. A.; Powell, A. K. *Inorg. Chem.* **1993**, *32*, 1502. (f) Glass, M. M.; Belmore, K.; Vincent, J. B. *Polyhedron* **1993**, *12*, 133. (g) Vincent, J. B.; Chang, H.-R.; Folting, K.; Huffman, J. C.; Christou, G.; Hendrickson, D. N. *J. Am. Chem. Soc.* **1987**, *109*, 5703.
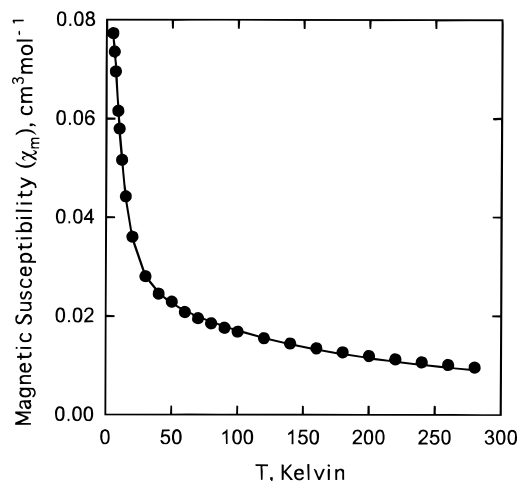
Figure 2. Plot of the molar magnetic susceptibility (χ_m) *vs* temperature for complex **1**. The solid line is a fit to the theoretical χ_m *vs* T expression for a [V$^{III}_3$] isosceles triangle; see text for the fitting parameters.

$S_T = 1$, 2, and 3 excited states at energies of $|2J|$, $|6J|$, and $|12J|$, respectively, above the ground state. The degeneracies of the S_T states are 1, 3, 2 and 1 for the $S_T = 0$, 1, 2, 3 states, respectively. Use of the above S_T, $E(S_T)$, and degeneracy values and the Van Vleck equation allows the derivation of a theoretical χ_M *vs* T expression for a V$^{III}_3$ equilateral triangle, which was used to fit the experimental χ_M *vs* T data. However, we could not obtain an acceptable fit of the experimental data to the theoretical expression for an equilateral triangle. Severe deviations between theoretical and experimental data were observed, particularly at lower temperatures where the predicted behavior indicated a maximum for χ_M at approximately 25 K, followed by a decrease at lower temperatures. The failure of χ_M for systems with a $S_T = 0$ ground state to decrease to low values is often due to the presence of a paramagnetic impurity whose susceptibility increases rapidly at low temperatures (Curie law), and a paramagnetic impurity term was therefore introduced into the theoretical χ_M *vs* T expression; allowing the molar ratio of paramagnetic impurity to be one of the fitting parameters gave improved fits but only when the impurity ratio was ~30%! Given the analytical and spectroscopic data on **1**, this was clearly an unreasonable and unrealistic fit.

In the literature, there are several reports of [M$_3$O(O$_2$CR)$_6$L$_3$]^z and related triangular metal complexes with trigonal symmetry whose magnetic behavior does not fit that expected for an equilateral triangle, i.e., a "one-J" model, but instead fits that expected for an isosceles triangle,[20-24] i.e., a "two-J" model, and the data for complex **1** were therefore analyzed as an isosceles system. The spin Hamiltonian for an isosceles triangle is given in eq 4, using for convenience the labeling scheme of

$$\hat{H} = -2J(\hat{S}_1 \cdot \hat{S}_2 + \hat{S}_1 \cdot \hat{S}_{2'}) - 2J'(\hat{S}_2 \cdot \hat{S}_{2'}) \qquad (4)$$

the C_2-symmetric cation of **4** in Figure 1, where $J = J_{12} = J_{12'}$ and $J' = J_{22'}$. This equation can be expressed in an equivalent form (eq 5) by use of the Kambe vector coupling methods[25]

(20) Jayasooriya, U. A.; Cannon, R. D.; White, R. P.; Stride, J. A.; Grinter, R.; Kearley, G. J. *J. Chem. Phys.* **1993**, *98*, 9303.

(21) Cannon, R. D.; Jayasooriya, U. A.; Wu, R.; arapKoske, S. K.; Stride, J. A.; Neilson, O. F.; White, R. P.; Kearley, G. J.; Summerfield, D. *J. Am. Chem. Soc.* **1994**, *116*, 11869.

(22) Duncan, J. F.; Kanekar, C. R.; Moh, K. F. *J. Chem. Soc. A* **1969**, 480.

(23) Long, G. J.; Robinson, W. T.; Tappmeyer, W. P.; Bridges, D. L. *J. Chem. Soc., Dalton Trans.* **1973**, 573.

(24) Caneschi, A.; Cornia, A.; Fabretti, A. C.; Gatteschi, D.; Malavasi, W. *Inorg. Chem.* **1995**, *34*, 4660.

(25) Kambe, K. *J. Phys. Soc., Jpn.* **1950**, *48*, 15.

$$\hat{H} = -J[\hat{S}_T{}^2 - \hat{S}_A{}^2 - \hat{S}_1{}^2] - J'[\hat{S}_A{}^2 - \hat{S}_2{}^2 - \hat{S}_{2'}{}^2] \quad (5)$$
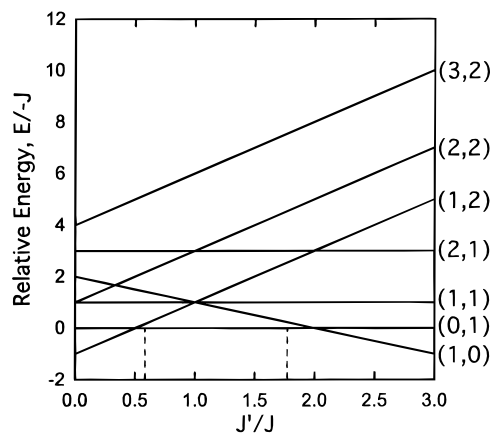
and the coupling scheme $\hat{S}_A = \hat{S}_2 + \hat{S}_{2'}$ and $\hat{S}_T = \hat{S}_A + \hat{S}_1$. This leads to the energy expression of eq 6 for the energies $E(S_T, S_A)$

$$E(S_T, S_A) = -J[S_T(S_T + 1) - S_A(S_A + 1)] - J'[S_A(S_A + 1)] \quad (6)$$

of the S_T states, where the constant terms involving S_1, S_2, and $S_{2'}$ and contributing equally to all states have been ignored. Use of eq 6 and the Van Vleck equation allows the theoretical χ_M *vs T* expression for a V^{III}_3 isosceles triangle ($S_1 = S_2 = S_{2'} = 1$; $S_A = 2, 1, 0$) to be derived. We now obtained an excellent fit of the experimental χ_M *vs T* data to this expression, shown as a solid line in Figure 2, with fitting parameters $J = -18.0(7)$ cm^{-1}, $J' = -10.4(4)$ cm^{-1}, and $g = 1.985$, no paramagnetic impurity term, and a temperature-independent paramagnetism (TIP) term held constant at 600×10^{-6} cm^3 mol^{-1}. These parameters indicate the ground state to be $S_T = 0$ arising from $S_A = 1$; in other words, (0,1) in the format (S_T, S_A). The excited states, in order of increasing energy, are (1,2), (1,1), (1,0), (2,2), (2,1), and (3,2), with the (1,2) first excited state only 5.6 cm^{-1} and the (1,1) second excited state 36.0 cm^{-1} above the (0,1) ground state.

Previous fits of the magnetic data for $[M_3O(O_2CR)_6L_3]^z$ and other triangular complexes have occasionally located both a local minimum and a global minimum,[23,24,26] and to explore whether such a situation also applies in the present work, we have generated a plot of the relative error for the fitting of the data as a function of J, J', and g; this did indeed show two distinct minima, one corresponding to the (global) minimum given above ($J = -18.0(7)$ cm^{-1}, $J' = -10.4(4)$ cm^{-1}, $g = 1.985$) and a second minimum at values of $J = -11.7$ cm^{-1}, $J' = -20.8$ cm^{-1}, and $g = 1.951$. The second fit is of only slightly higher relative error, and it became of importance to assess the nature of the spin state manifold for the second set of J, J', and g values: in fact, the latter also indicate a (0,1) ground state but the first excited state is now the (1,0) state at 5.2 cm^{-1} above the ground state. Both the global and local minima thus indicate a $S_T = 0$ ground state for complex **1**.

We are aware of only one previous magnetochemical study of a triangular V^{III}_3 complex; Allin and Thornton[27] fitted higher temperature (98–293 K) data to a one-*J* model and estimated J to be -15 cm^{-1} for a compound suspected to be $[V_3O(OAc)_7-(HOAc)]_\infty$, an AcO-bridged polymer. This value is very close to the average (-15.5 cm^{-1}) obtained in the present work. In a general manner, the exchange interactions within a M_3 triangular system comprising three $S = 1$ spin centers have been addressed by Kahn[28] in his consideration of competing exchange interactions and spin frustration effects within such complexes. Of relevance here is the variation of spin state energies in an isosceles triangle ($J \neq J'$) as a function of the J'/J ratio, i.e., the relative magnitude of the two exchange interactions: for a triangular array of three $S = 1$ spins in which both J and J' are antiferromagnetic (i.e., negative), it is not possible for the three spins to all be aligned antiparallel to each other, and the precise spin alignments (and the resultant ground state) thus become sensitive to the relative magnitude of the two "competing" exchange interactions, i.e., the J'/J ratio. A plot of the spin state energies as a function of J'/J can be derived using eq 6;

(26) McCusker, J. K.; Jang, H. G.; Wang, S.; Christou, G.; Hendrickson, D. N. *Inorg. Chem.* **1992**, *31*, 1874.
(27) Allin, B. J.; Thornton, P. *Inorg. Nucl. Chem. Lett.* **1973**, *9*, 449.
(28) Kahn, O. *Molecular Magnetism*; VCH Publishers, Inc.: New York, 1993; Chapter 10.

Figure 3. Plot showing the variation in the energies of the spin states of a $[V^{III}_3]$ complex as a function of the J'/J ratio. The spin states are labeled in the format (S_T, S_A). The dashed lines at $J'/J = 0.58$ and $J'/J = 1.78$ indicate the global and local minima, respectively, referred to in the text.

this has been shown elsewhere by Kahn[28] but is also presented in Figure 3 for convenience. The ground state is the (0,1) state for J'/J values from 0.5 to 2.0, with the (1,2) and (1,0) states becoming the ground states at J'/J values of <0.5 and >2.0, respectively. The ratio of J and J' for the global minimum ($J'/J = 0.58$) gives the spin manifold indicated by the dashed line on the left of Figure 3, close to the crossover point at which the ground state changes. Interestingly, the local minimum ($J'/J = 1.78$) shown on the right of Figure 3 is close to the other crossover point.

The relative magnitude of the competing J and J' exchange interactions in **1** ($J'/J = 0.58$) leads to the (0,1) ground state, which can be represented diagrammatically as
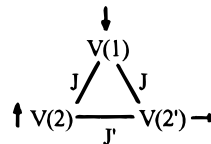
atoms V(2) and V(2$'$) are, of course, equivalent by symmetry, and this diagram is thus to be interpreted as showing that spins S_2 and $S_{2'}$ align neither perfectly parallel ($S_A = 2$) nor antiparallel ($S_A = 0$) but in an intermediate manner to give a resultant $S_A = 1$, which aligns antiparallel to S_1 to give the observed $S_T = 0$ ground state of **1**.

^{1}H NMR Spectroscopy. The solution properties of the $[V_3O(O_2CR)_6L_3]^+$ complexes were investigated by ^{1}H NMR spectroscopy in CD$_3$CN or CD$_2$Cl$_2$, depending on solubility. The data for complexes **1**–**8** are collected in Table 4, and a representative spectrum of complex **1** is shown in Figure 4. It is important to comment first on the small signals noticeable at the base of the main peaks and the presence of free py (marked ×); our first thought was that our sample was impure, but recrystallized material gave the same spectrum. Further, these small signals (and those for free py) slowly grow with time and after several hours have intensities not much smaller than the (initial) main peak. We interpret this behavior as indicating slow substitution of the terminal py groups: this behavior is also observed for **2**–**4** in CD$_3$CN and for **5**–**8** in CD$_2$Cl$_2$, but the small signals are less apparent for the latter, consistent with the better donor strengths of the methyl-substituted pyridines. In CD$_3$CN, the py groups are presumably being replaced by solvent and/or water groups, whereas in CD$_2$Cl$_2$ it is presumably water only. Addition of an excess of pyridine-d_5 to an aged solution of **1** in CD$_3$CN causes a dramatic decrease in the

Table 4. ^{1}H NMR Data at ~23 °C for [V$_3$O(O$_2$CR)$_6$L$_3$](ClO$_4$) Complexes **1**–**8**

	R	L	δ(R), ppm^{c,d}	δ(L), ppm^{c,d}
1^a	Me	py	46.4	−16.4 (*o*), 11.4 (*m*), −2.9 (*p*)
2^a	Me	pic	46.0	−15.7 (*o*), 11.2 (*m*), (12.7) (*p*)
3^a	Me	lut	46.1	−16.2 (*o*), (−1.6) (*m*), −2.0 (*p*)
4^a	Et	pic	55.8 (CH$_2$), 0.8 (Me)	−17.7 (*o*), 11.6 (*m*), (15.4) (*p*)
5^b	C$_6$H$_4$-*p*-OMe	pic	0.4 (*o*), 8.1 (*m*), (5.1) (*p*)	−18.1 (*o*), 12.0 (*m*), (16.2) (*p*)
6^b	Ph	pic	0.5 (*o*), 9.1 (*m*), −0.4 (*p*)	−16.6 (*o*), 11.6 (*m*), (14.9) (*p*)
7^b	C$_6$H$_3$-*m*-Me$_2$	pic	0.2 (*o*), (−0.5) (*m*), −0.9 (*p*)	−16.6 (*o*), 11.6 (*m*), (15.2) (*p*)
8^b	C$_6$H$_4$-*p*-Cl	pic	0.2 (*o*), 9.2 (*m*)	−16.2 (*o*), 11.5 (*m*), (14.1) (*p*)

^{a} In CD$_3$CN. ^{b} In CD$_2$Cl$_2$. ^{c} ±0.1 ppm, *vs* TMS; numbers in parentheses refer to a Me group at that position. ^{d} Chemical shifts upfield of $\delta = 0.00$ are negative. *o* = ortho; *m* = meta; *p* = para.

O$_2$CC$\underline{H}_3$
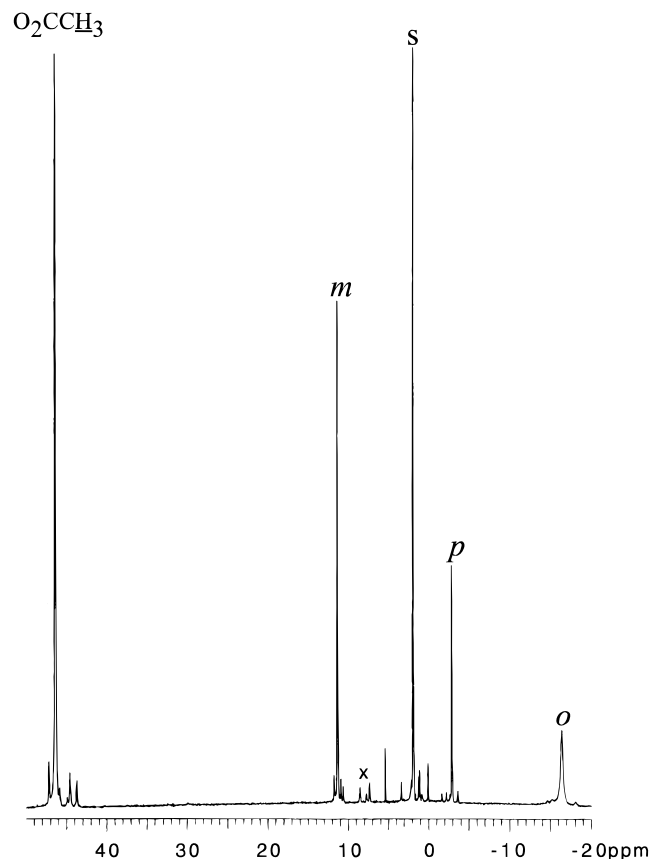
Figure 4. ^{1}H NMR spectrum of complex **1** in CD$_3$CN at ~23 °C: solvent impurity (S) and free py (×) are indicated.

intensities of the side signals, the latter becoming comparable with those in Figure 4 for a freshly-prepared solution. Thus, the loss of py is reversible, and the substitution is summarized in eq 7, assuming for convenience that only H$_2$O is involved.

$$[\text{V}_3\text{O}(\text{O}_2\text{CR})_6(\text{py})_3]^+ + x\text{H}_2\text{O} \rightleftharpoons$$
$$[\text{V}_3\text{O}(\text{O}_2\text{CR})_6(\text{py})_{3-x}(\text{H}_2\text{O})_x]^+ + x\text{py} \quad (7)$$
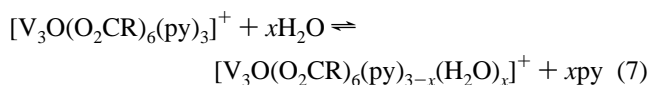
The spectrum for complex **1** in Figure 4 shows four resonances assignable to the [V$_3$O(O$_2$CMe)$_6$(py)$_3$]$^+$ cation: the indicated assignments are based on the relative integration ratios (9:6:6:3), the peak broadnesses (r^{-6} dependence, where r is the

distance to the paramagnetic centers), and the spectra of complexes **2**–**8**, possessing other carboxylate groups and substituted py rings (*vide infra*). The MeCO$_2^-$ resonance of **1** is paramagnetically shifted far downfield at $\delta = 46.4$ ppm, whereas the py resonances are shifted both upfield (*o*- and *p*-hydrogen resonances) and downfield (*m*-hydrogen resonance). A single set of MeCO$_2^-$ and py resonances is consistent with effective D_{3h} symmetry for the cation in solution and thus the retention of its trinuclear structure on dissolution in MeCN.

The essentially C_{4v} local symmetry at each V^{III} center and the short V−O(3) distances to the central O^{2-} ion likely result in a b$_2$(xy)^1 e(xz,yz)^1 electronic configuration at each V^{III} ion (taking the N−V−O(3) axis as the z axis, and the equatorial V−O bonds as the x, y axes). Thus, all unpaired spin density is in d$_\pi$ orbitals, and contact shift contributions to the hydrogen paramagnetic shifts should be primarily by π-spin-delocalization mechanisms.[29] This is consistent with the observed shifts in Figure 4: π-symmetry overlap of the b$_2$(xy) orbital with the carboxylate π system will result in direct delocalization of positive (parallel) spin density from the metal into the −CO$_2$ π system and then onto the Me group *via* the π-symmetry orbitals of the Me fragment; parallel spin density at the Me hydrogen atoms leads to a downfield contact shift. Similarly, π-symmetry overlap between the e(xz,yz) orbitals and the py π system leads to direct delocalization of parallel spin density from the V onto the *o*- and *p*-positions of the py ring; this results in antiparallel (negative) spin density at the *o*- and *p*-H nuclei from spin polarization effects and gives upfield paramagnetic shifts of these NMR resonances. Similar spin polarization effects gives parallel (positive) spin density at the *m*-H nuclei and resulting downfield shifts. Thus, the observed alternating upfield−downfield−upfield shifts of the py hydrogen resonances in **1** are indicative of a dominant π−spin-delocalization mechanism for the contact shifts. This is also supported by the spectra of **2**–**8**. In particular, the substitution of Me for H at the *m*- or *p*-positions of the py ring (**3** or **2**, respectively) changes the sign (direction) of the paramagnetic shifts of the hydrogen resonances for these positions; this is as expected if the contact shifts are dominated by a π-spin-delocalization mechanism.[29]

The same alternation in sign is seen around the Ph group of the benzoate complex **6**, supporting π-spin delocalization and the previous interpretation for the acetate group of **1**. Me/OMe-for-H substitution at *m*- and *p*-positions again changes the signs of the shifts. Note that all shifts for the benzoate group (and its substituted derivatives) are smaller than for the py-based rings, probably due to free rotation of the Ph ring which decreases the influence of the π-spin-delocalization mechanism. In addition, there are likely also contributions to the hydrogen paramagnetic shifts from dipolar (pseudocontact) contributions, but it is difficult to assess their relative importance with the present data except to say that they appear to be minor contributions relative to the π-contact shifts.

Electrochemical Studies. The electrochemical properties of selected complexes have been investigated in CH$_2$Cl$_2$; the pic complexes **2**, **4**, **5**, **6**, and **8** were chosen to minimize problems with terminal ligand exchange. The complexes were investigated by cyclic voltammetry (CV) and differential pulse voltammetry (DPV), and the results are collected in Table 5. The complexes all exhibit a reversible one-electron reduction, a second, irreversible reduction, and an oxidation that appears reversible only at higher scan rates, suggesting a slow subsequent transformation. The first reduction occurs at a quite low potential (<-1.4 V *vs* ferrocene), consistent with generation

(29) *NMR of Paramagnetic Molecules*; LaMar, G. N., Horrocks, W. DeW., Jr., Holm, R. H., Eds.; Academic Press: New York, 1973.

Table 5. Electrochemical Data[a,b] for $[V_3O(O_2CR)_6(pic)_3](ClO_4)$ Complexes

R	redn 1[c]	redn 2[d]	oxidn
Me (**2**)	−1.48	−1.7	0.58
Et (**4**)	−1.61	−1.9	0.47
p-OMe-Ph (**5**)	−1.53	−1.8	0.46
Ph (**6**)	−1.40	−1.7	0.67
p-Cl-Ph (**8**)	−1.32[d]	n.o.[e]	0.77

[a] V *vs* ferrocene; values are DPV peak potentials. [b] 0.001 M in 0.1 M NBu$^n_4$ClO$_4$ in CH$_2$Cl$_2$. [c] Reversible. [d] Irreversible. [e] n.o. = not observed.

of a strongly-reducing, V^{II}-containing species, as summarized in eq 8. The complex $[V_3O(O_2CMe)_6(py)_3]$ has been prepared

$$[V_3O(O_2CR)_6(pic)_3]^+ + e^- \rightarrow [V_3O(O_2CR)_6(pic)_3] \quad (8)$$
$$(3V^{III}) \qquad\qquad\qquad (V^{II},2V^{III})$$

and structurally-characterized by others,[13a] confirming its V^{II}, 2V^{III} oxidation level.

Conclusions

The reaction of VCl$_3$(THF)$_3$, NaO$_2$CR, and py derivatives in organic solvents provides a convenient route to large quantities of $[V_3O(O_2CR)_6L_3]^+$ salts, facilitating physical and spectroscopic study for the first time. Structural characterization of complex **4** confirms the triangular structure of material via this procedure. The core structure is retained on dissolution in MeCN or CH$_2$Cl$_2$, permitting NMR and electrochemical characterization. The complexes exhibit antiferromagnetic exchange interactions between the paramagnetic V^{III} centers, and the magnetic susceptibility *vs* temperature behavior may be modeled using an isosceles (two-*J*) coupling scheme.

The ready formation and stability of these trinuclear species suggest their formation on reduction and partial deoxygenation of vanadyl carboxylates during crude oil hydro-treating should be entertained. The reactions of the $[V_3O(O_2CR)_6L_3]^+$ species with S-containing reagents such as H$_2$S to model sulfiding processes to give V/S complexes and ultimately V$_2$S$_3$ and V$_3$S$_4$ now become of interest, and these will be facilitated by the high-yield routes to $[V_3O(O_2CR)_6L_3]^+$ salts reported in this work. Other reactions of these trinuclear complexes are also of interest; one such reaction between $[V_3O(O_2CEt)_6L_3]^+$ generated *in situ* and 2,2′-bipyridine (bpy) was recently shown to yield the new complex $[V_4O_2(O_2CEt)_7(bpy)_2](ClO_4)$.[12] This reaction suggests that the $[V_3O(O_2CR)_6L_3]^+$ species may represent a rich new source of V^{III} complexes of various nuclearities, and studies along these lines are in progress.